

Fruit Quality Sensing via Image Processing

ECE 298 Thesis

Andrew He

Advisor: Yasaman Ghasempour

Submitted in partial fulfillment of the requirements for the degree of Bachelor of
Science in Engineering Department of Electrical and Computer Engineering
Princeton University

December 4, 2023

I hereby declare that this Independent Work report
represents my own work in accordance with University
regulations. - Andrew He

Andrew He

Fruit Quality Sensing via Image Processing

Andrew He

Abstract

The efficient and precise assessment of fruit ripeness metrics holds immense potential for transforming the agricultural industry, leading to reduced waste and optimized resource utilization. However, current sensing methods suffer from limitations such as slow processing, reduced accuracy, and lack of scalability. In this paper, we propose a novel approach that leverages advanced imaging techniques to rapidly develop comprehensive ripeness models applicable to various fruits. The core concept revolves around monitoring and analyzing changes in color, enabling the creation of accurate ripeness models. By effectively mapping the surface color to the sugar content of fruits, a crucial indicator of ripeness, this approach can be seamlessly integrated with other technologies to enhance the development of robust ripeness models.

Acknowledgements

I would like to first thank my thesis advisor Professor Yasaman Ghasempour for her guidance and insight for this project. Her knowledge and funding were especially crucial for this project and I thank her for being both an advisor and a mentor to this project.

I would also like to thank Atsutse Kludze for assisting me greatly throughout the project in experimentation, processing, and writing as he was both quickly responsive and insightful. I would also like to thank the Smart Wireless Agile Networks (SWAN) lab for their support and funding for this project.

Finally, I would like to thank Professor Wysocki for being my second reader as well as the Department of Electrical and Computer Engineering for allowing me to fulfill my passion for research early in my time as a student here.

Contents

Abstract	2
Acknowledgements	3
1 Introduction	6
1.1 Thesis	7
2 Primer	9
2.1 Cycle of Fruit Ripening	9
2.1.1 Ripeness Metrics	10
2.2 Existing Solutions and Their Limitations	11
2.2.1 Why Imaging?	13
3 Experimental Setup and Results	15
3.1 Design and Experimental Setup	15
4 Evaluation	18
4.1 Imaging Results	18
4.2 Initial Feasibility	20
4.3 Brix Model	22
4.4 Dry Matter Model	23
4.5 Ripeness Metric Estimation Performance and Evaluation	25

5	Discussion and Future Work	27
5.1	Discussion	27
5.2	Future Work	28
6	Conclusion	30
A	Appendix	31
A.1	Engineering and Industrial Standards	31
A.2	Image Processing	33

Chapter 1

Introduction

As the global population continues to grow, the demand for agricultural resources has increased accordingly [16]. To meet these demands, farming has significantly increased its output to sustain the current population, with the total farm output in the United States tripling since 1948 and 2019 [2]. However, according to the United Nations, nearly half of all fresh produce is wasted annually [44]. With the current production rates, this amounts to approximately \$48.3 billion in wastage losses within the United States alone [3].

An alternative focus to solely increasing production is reducing the wastage in the production process, which can contribute to higher yield rates [34]. This high level of inefficiency can be attributed to the lack of accurate assessment methods for products such as fruits and vegetables. Current processes rely on methods from sample testing, where only small quantities are tested to represent the entire batch [56], to being inaccurately inspected through humans [27]. Consequently, large batches of products are often discarded due to the inability to simultaneously assess the quality of all agricultural products passing through a processing plant [18]. However,

implementing accurate testing for each fruit using the current methods would result in infeasible processing costs that would overshadow the production costs. The significant inefficiencies in the food industry, coupled with the high costs of harvesting, transportation, and processing, have contributed to costly operations and the inaccessibility of high-quality calories in developed countries [28]. Therefore, the development of an automated, non-invasive process to accurately determine food quality on a large scale remains an open research topic.

1.1 Thesis

However, the ripening process is an intricate and complex process, consisting of many different chemical reactions. As such in order to develop a ripeness model, certain applicable metrics to describe the ripening process must be implemented such as measurements of the concentrations of key molecules (such as sugar and water) or weight/physical measurements. This paper aims to propose a solution to this issue by introducing an end-to-end non-invasive system for scalable fruit quality and ripeness estimations (Figure 1.1). Our approach involves tracking the changes in the exterior color of fruits and relating them to key metrics such as Brix [50] (sugar content) and Dry Matter [37] (non-water mass). We believe that there are distinct alterations in the spectral reflectance of fruits that can be assessed using commercially available equipment. As many fruits share common pigments, our end-to-end system demonstrates the feasibility of rapidly developing unique models that aims to provide accurate and reliable fruit ripeness estimations.

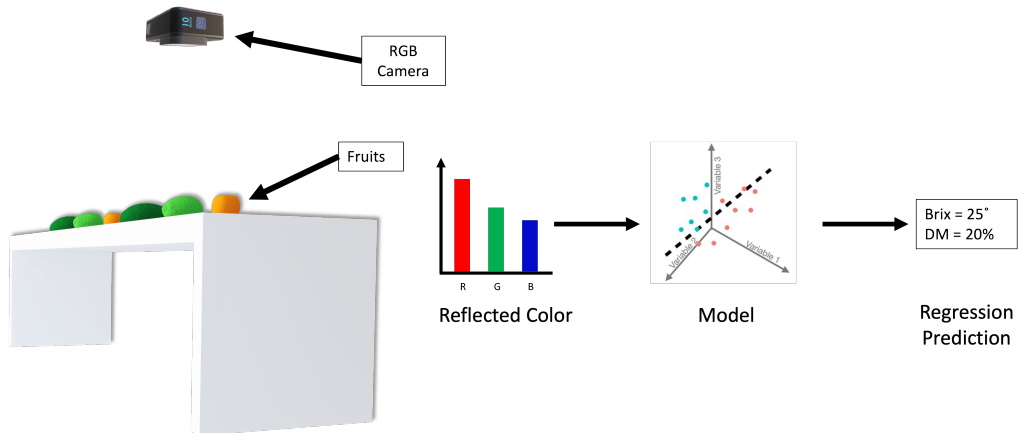


Figure 1.1: This figure shows an end-to-end image sensing system that extracts the color characteristics of the fruit to develop a quantitated ripeness prediction in Brix and Dry Matter.

Chapter 2

Primer

In this section, we introduce the metrics used for quantifying ripeness. In addition, we demonstrate why current methods are insufficient and why colors can provide an accurate estimation of the stage of fruit ripeness.

2.1 Cycle of Fruit Ripening

The ripening process of fruits can be categorized into distinct regulatory mechanisms that encompass maturation, senescence, and a transitional stage where the fruit undergoes ripening after being separated from the host plant [47, 48]. Climacteric fruits, such as apples, avocados, and persimmons, continue to ripen after detachment from the host plant, making it challenging to manage their ripening during transportation and distribution along the supply chain [40]. In contrast, non-climacteric fruits, including citrus fruits, strawberries, and grapes, halt their ripening process once separated from the host plant [40].

To track the ripening cycle of fruits, this paper focuses specifically on the mat-

uration component in climacteric fruits. However, monitoring fruit maturity is a complex process that involves multiple metrics to quantify ripening and determine different maturity stages in fruits. These metrics include properties such as Dry Matter, Brix, and Surface Coloration [43]. Each metric provides valuable information about the ripening process and can be used to assess the maturity of fruits in detail.

2.1.1 Ripeness Metrics

To accurately determine the ripeness stage of fruits, it is necessary to simplify the complex physiological process. The industry commonly utilizes three metrics to assess fruit ripeness:

- **Degrees Brix (commonly referred to as Brix):** This metric measures the sugar content of fruits in terms of percentage concentration and varies between fruits (monosaccharides, disaccharides, and oligosaccharides, such as sucrose, fructose, etc.)[30]. Brix changes over time in most fruits as they ripen as fruits store energy in the form of short-chain carbohydrates. For instance, a ripe persimmon typically has a Brix value ranging from 24 to 27.5 [13], indicating a total sugar concentration of 24% to 27.5%. Sugar content directly impacts the taste and is easily noticeable by consumers, making it a suitable indicator of ripeness.
- **Dry Matter (DM):** This metric describes the solid components of fruits excluding water. For example, a ripe apple may have a Dry Matter metric of 20%, indicating that 20% of its mass consists of non-water molecules. Dry Matter encompasses various non-water molecules, including carbohydrates, fiber, and lipids, that change over time corresponding to the ripening process. This consolidates multiple potential ripeness indicators into a single metric

[17].

- **Surface Color:** The process of fruit ripening has involved ripeness that involves several physiological and organoleptic alterations [54]. Since many of the chemicals that control the ripening process also function as pigments, this causes fruits such as apples and avocados to change their colors throughout the ripening process [38]. For example, most fruits such as persimmon start out as green due to chlorophyll giving them the green color [57]. As they mature, the chlorophyll deteriorates and is replaced by pigments such as orange carotenoids and blue anthocyanins [49]. These serve as antioxidants that protect the fruit from oxidizing and spoiling [32]. Tracking the change of the pigments through color can provide a metric to measure ripeness.

2.2 Existing Solutions and Their Limitations

Tracking these metrics to quantitate the various ripeness stages of fruits has been an incentive for various aspects of the supply chain, from growers to shippers and distribution centers. As such, there already exist various solutions to test for the metrics listed above listed below:

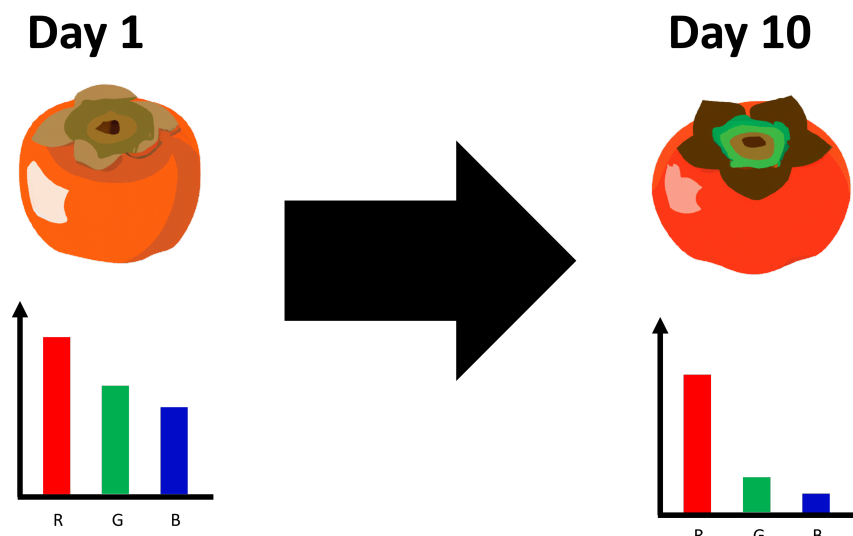
- **Sensory Evaluation:** This involves assessing ripeness through trained individuals who evaluate the tastes, colors, and textures of a small number of fruits. However, this method lacks scalability and is prone to human error [7].
- **Firmness Measurements:** This utilizes physical instruments to perform texture analysis. Although it reduces human bias, it is not very accurate and lacks scalability [46].
- **Sugar Content Analysis:** This utilizes instruments capable of refractometry

etry or high-performance liquid chromatography (HPLC) to measure sugar content. This is through physical/optical methods in order to segment the sugar concentrations. While portable and field-usuable, this method is slow, and each fruit tested must be destroyed [15].

- **Aroma/Ethelyne Gas Analysis:** This involves instruments like gas chromatography-mass spectrometry (GC-MS) to track volatile chemicals released during the climacteric phase of fruit ripening. It is suitable for measuring large batches of fruits in distribution processes but cannot evaluate individual fruits and is limited to specific distribution vectors [39].
- **Near Infrared (NIR Spectroscopy):** This optical evaluation method involves transmitting NIR pulses into the fruit and measuring the reflection. It is non-destructive and widely used in the fruit industry for ripeness evaluation across the supply chain [51]. NIR sensors can be categorized into two types:
 - **Inline Sensors:** These large, immobile installations are placed along sorting lines and can process fruits on a large scale with quick evaluation times. However, they sacrifice accuracy and have limited installation cases, leading to unnecessary fruit rejections [29].
 - **Portable Sensors (lab grade):** These small sensors can be deployed in the field and evaluate fruits individually with a high degree of accuracy. This is due to the extended length allowed for spectroscopy, allowing for more accurate results [11]. However, using them is a slow and manual process, reducing scalability. [c]

2.2.1 Why Imaging?

Imaging has emerged as a popular method for ripeness detection, owing to the irreversible nature of fruit ripening, which is governed by changing concentrations of organic molecules that also serve as pigments [59]. Fruits have evolved a symbiotic relationship with animals, and alterations in reflectance within the visible light spectrum offer a potential means of tracking ripeness stages in fruits [42]. For instance, many fruits initially exhibit green coloration due to chlorophyll pigmentation [12]. As the fruits mature and photosynthesis productivity declines, the green pigmentation diminishes, allowing other pigments like orange carotenoids and blue anthocyanins to reflect more light (Figure 2.1) [35]. Monitoring changes in imaging may facilitate the development of models capable of accurately predicting fruit stages by visually assessing pigment concentrations.



Example: As persimmons ripen, they change from a light orange color to a darker red. As such, we can correlate the change in its RGB color to ripeness.

Figure 2.1: This figure shows how the reflectances of the colors change in a Persimmon over time.

However, current literature on ripeness sensing using imaging primarily relies on

machine learning for image classification [14, 22, 45]. While these complex models may effectively predict the ripeness of specific fruits, they struggle to provide accurate generalizations to fruit ripeness for offering explanations on the overall mechanisms for ripeness. The use of classification-based approaches presents inherent challenges related to overfitting, as an excessive number of parameters can lead to data overfitting [6]. Consequently, the lack of transparency resulting from the high complexity of machine learning models hinders their interpretability [52]. Additionally, machine learning models require extensive and diverse datasets to be viable [9] and to mitigate potential bias amplification [33]. Consequently, the development of image classifications becomes a resource-intensive and time-consuming task that is beyond the reach of many unless substantial resources are available for model training. Thus, an alternative approach is needed to circumvent the challenges posed by training "black-box models" in machine learning, which are inherently difficult to interpret.

This paper presents a methodology focusing on identifying visual cues associated with fruit ripening. Specifically, the analysis is limited to the color ranges typically captured by cameras, namely Red, Green, and Blue (560nm, 530nm, 430nm). To develop our model, we adopt a Partial Least Squares Regression (PLSR) approach due to its robustness and compatibility with existing image classification models. The PLSR model enables us to establish a multivariate regression that minimizes the discrepancy between predicted and actual values, hence the term "least squared" [55]. By utilizing PLSR, we can specifically define the target characteristics we aim to model, in this case, color [20]. This dimensionality reduction technique allows for efficient linkages to the input data elements, improving the reliability of our model [23]. Furthermore, the image model reduces the reliance on extensive training data typically required by machine learning models [10]. As a result, our approach facilitates the direct identification of factors influencing ripeness metrics.

Chapter 3

Experimental Setup and Results

In this section, we explain the design methodology, and experimental setup, and illustrate the results.

3.1 Design and Experimental Setup

For this experiment, three fruits were selected as the focus: Avocado, Green Apples, and Persimmon. These fruits are climacteric and widely consumed worldwide, exhibiting varying rates of color changes that correspond to different ripeness metrics such as Brix and Dry Matter. Each fruit type consisted of ten fruits with closely matched Brix/Dry Matter values, within a 2% range, and all fruits were unripe at the beginning of the experiment.

To identify the relevant elements for constructing our model, we created an environment that closely mimicked a real-world setting using a conveyor belt setup (Fig 3.1). A white Styrofoam background was chosen, and the lighting conditions were carefully controlled to maintain consistency across the collected results. The

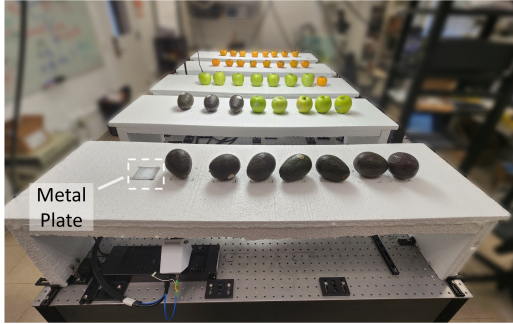


Figure 3.1: All 30 fruits (Avocados, Apples, Persimmon) laid out on Styrofoam. The position was fixed for 10 days.



Figure 3.2: Camera mount location (GoPro Hero 10). RAW images are captured every 12 hours, synchronizing with the NIR sensor measurement times, to capture color data.

fruits were securely positioned and remained fixed for ten days, with measurements taken at 12-hour intervals. Simultaneously, two cameras equipped with ultra-wide lenses captured RAW images, allowing us to obtain comprehensive pictures of the entire area for subsequent analysis (Fig 3.2). This process resulted in a total of 20 pictures and measurements for all 30 fruits (Fig 3.3).

To establish baseline measurements, we employed the F750 Food Quality Sensor [26], which is a commercially available tool widely recognized as the industry standard for non-invasive and accurate Brix and Dry Matter measurements. This device utilizes NIR Spectroscopy and is pre-calibrated by the manufacturer specifically for the fruits under investigation. It provides precise results (Figure 3.4) for Dry Matter in Green Apples and Avocados and Brix in Persimmon and Avocado [19]. However, as mentioned earlier, the sensor's effectiveness is limited when testing large batches due to the need for proximity to the fruit for an extended period (Fix 3.3). Nevertheless, its non-invasive nature is essential for our experiments, ensuring minimal external environmental influence on the fruits.



Figure 3.3: Establishing baseline measurements for a Persimmon. The sensor must be placed near the contact range of the fruit, requiring around 2-3 minutes per fruit.



Figure 3.4: Product Picture of F750 produce quality meter is from Felix Instruments [1].

Chapter 4

Evaluation

This section will develop and evaluate the models generated to represent the fruit. All evaluations are based on a 10-day time span with 12-hour photo and NIR intervals with the median results at each interval taken to reduce error.

4.1 Imaging Results

Upon concluding the ten-day experiment, all fruits exhibited the expected changes. However, these color changes proved challenging for the human eye to discern, as indicated by Figure 4.1, which demonstrates negligible alterations in the fruit's skin physiology.

This difficulty in perception can be attributed to human color perception. To account for this, we employed Delta E values, utilizing the LAB color space, which mimics the human eye [58]. By tracking changes on a delta E scale, where a value of 0 represents identical images and 100 represents completely different images, we observed that the maximum Delta E values for Persimmon and Green Apples ranged

between 0 and 5 (Figure 4.2).

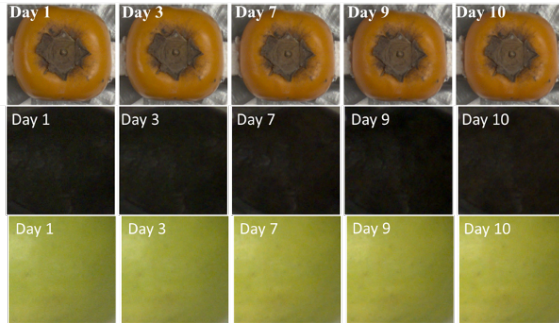


Figure 4.1: Pictures of sample fruits for a 10-day span.

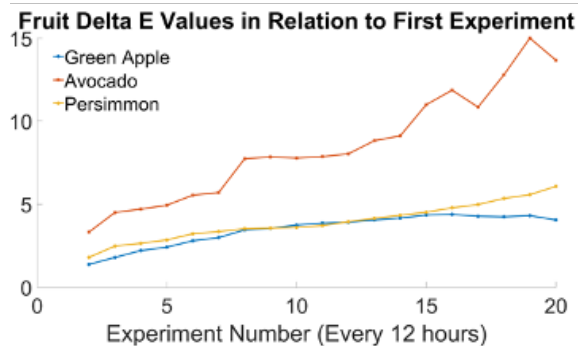


Figure 4.2: Delta E values in comparison to the first picture over time.

In terms of human color detection, these changes are considered minimal, rendering the color differences seemingly insignificant. However, a comprehensive analysis of the overall changes, considering correlations in terms of SSIM or structural similarity [5], reveals a significant change (Fig 4.3) characterized by a clear linear trend. Therefore, the extracted results demonstrate a linear relationship between color and ripeness, suggesting the potential for developing a linear model linking ripeness to color.

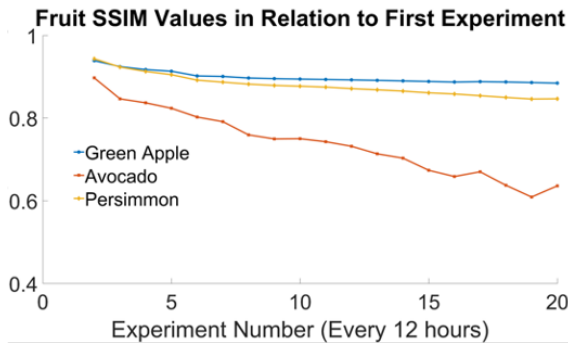


Figure 4.3: SSIM value in comparison to the first picture over time (eg. 0.9 means 90% similarity).

4.2 Initial Feasibility

The primary objective of this experiment is to demonstrate that the external physiological surface of the fruits undergoes a measurable linear change over time. To validate this hypothesis, a feasibility test will be conducted. The test aims to identify any significant changes observed in the raw analysis of the color components. Initially, a 200x200 pixel grid is assigned to each fruit, covering the entire field of view. To assess the impact of each color component, Red, Green, and Blue masks are created, and the Structural Similarity Index (SSIM) is measured over time by comparing the subsequent images with the initial ones. This crucial initial step enables us to identify any significant trends in the data and find the likelihood of developing a model with sound components and rationale (Fig 4.4). Based on the analysis depicted in Figure 4.4, it is evident that the blue reflectance in all fruits has experienced a substantial change compared to other wavelengths. This finding is highly encouraging as it aligns with the hypothesis that certain visible light frequencies directly correlate with the ripening process. Consequently, utilizing individual colors as components, rather than employing all colors together in a machine-learning model, emerges as a promising approach to make a generalizable and effective model.

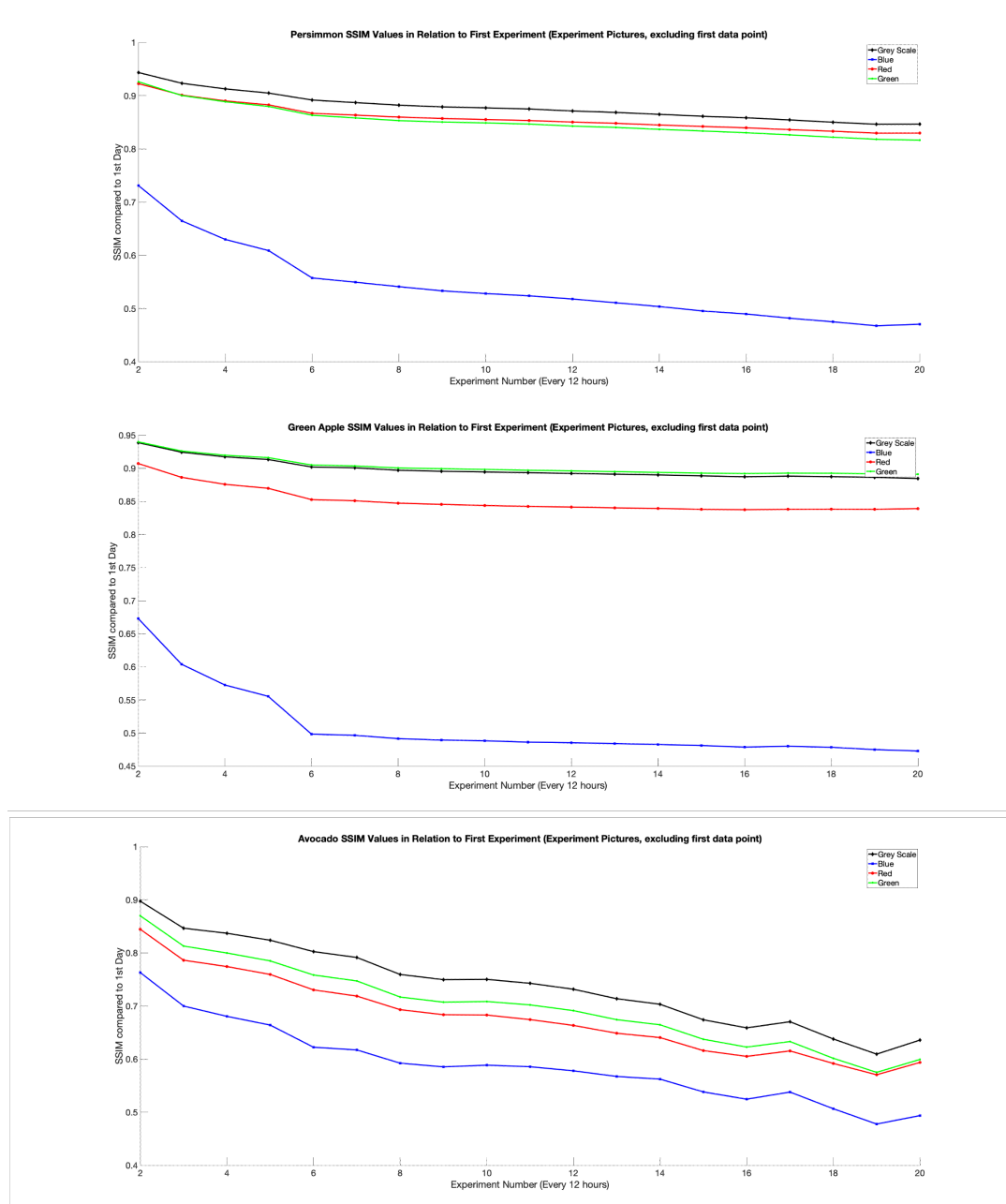


Figure 4.4: Structural Similarity Index across all colors and overall color change (greyscale). All fruits exhibit a significant change in blue reflectance.

4.3 Brix Model

To understand the relationship between reflectance and Brix values (percentage sugar content to total mass), a comparison was made between the reflectance values and the ground truth established by the Felix F750 Food Quality Sensor. However, due to limitations in the provided calibration data from the manufacturer [1], the sensor was only capable of measuring the Brix content of Green Apple and Persimmon. The collected Brix data over a 10-day period, represented in Figure 4.5, shows the values plotted against time in hours. It can be observed that the Brix values reach a plateau at 9 days for Persimmon and 5 days for Green Apples. These correspond closely to the change in the blue reflectances from Figure 4.3 plateausing at roughly the same time period.

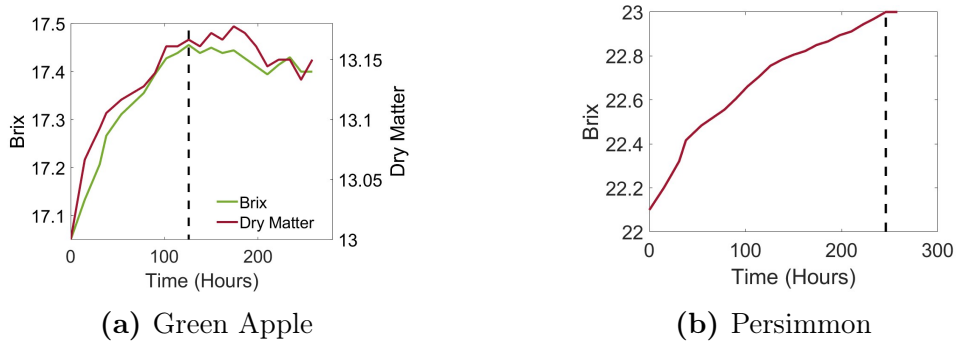


Figure 4.5: Measured Trends in Brix and Dry Matter. The figure shows the Brix values of both the Green Apple and the Persimmon in 12 hour intervals over 10 Days

Using the data from Figure 4.4 to construct a Brix model, we find the Blue reflectance has the highest correlation out of any wavelength in both of the PLS regressions constructed from the RGB masks and greyscale (Fig 4.6). This is further demonstrated by the Blue reflectance value accounting for nearly 76% and 82.8% of the correlation, demonstrating that it exhibits the highest impact on the model prediction results (Fig 4.7).

Estimated Coefficients:				
	Estimate	SE	tStat	pValue
(Intercept)	19.219	1.8342	10.478	1.4293e-08
x1	5.4845	6.7776	0.80921	0.43026
x2	-6.6831	7.2427	-0.92274	0.36985
x3	-0.84791	0.8847	-1.0537	0.30768

Estimated Coefficients:				
	Estimate	SE	tStat	pValue
(Intercept)	39.123	5.424	7.2149	2.0619e-06
x1	-9.4478	16.644	-0.56764	0.57816
x2	-13.724	9.2074	-1.4985	0.15554
x3	6.318	2.2415	2.8186	0.012357

(a) Green Apple

(b) Persimmon

Figure 4.6: This figure shows the PLS Regression results for both Green Apple and Persimmon. x1, x2, x3 represent Red, Green, and Blue respectively. Note that blue (x3) has the lowest P-value both cases.



Figure 4.7: This figure shows the PLS contribution of the components. In both cases, the first component is the Blue contribution. Hence the intersection with the Y axis represents the contribution of the Blue reflectance.

4.4 Dry Matter Model

Having established the relationship between reflectance and Brix values, a similar comparison can now be conducted for Dry Matter (percentage of non-water mass). However, due to additional limitations in Dry Matter measurements from the sensor provided by the manufacturer of the Felix F750 sensor [1], it is only possible to establish a Dry Matter relationship for Avocados and Green Apples. Figure 4.8 illustrates the trend observed in Dry Matter for these fruits. Green Apple exhibits a similar pattern as observed in Brix, with a plateau at 5 days. On the other hand, Avocado reaches a peak at approximately 5 days and then experiences a decline shortly thereafter.

The construction of a Dry Matter model based on the data presented in Figure 4.4 reveals a significant difference compared to the Brix model. While the correlation

between green apple and Dry Matter remains similar, indicating a strong relationship between sugar content and Dry Matter percentage, there is a notable shift in the trend from the PLSR model with regards to Avocado. In the PLS components shown in Figure 4.9 (p-value), it is evident that Avocado does not have equivalent effects from all bands on the resulting Dry Matter percentage value. Specifically, Avocado exhibits a correlation of 40% to the resultant Dry Matter. In contrast, the correlation between Green Apple and Brix remains almost unchanged, with an 83.2% correlation to Dry Matter (Fig 4.10).

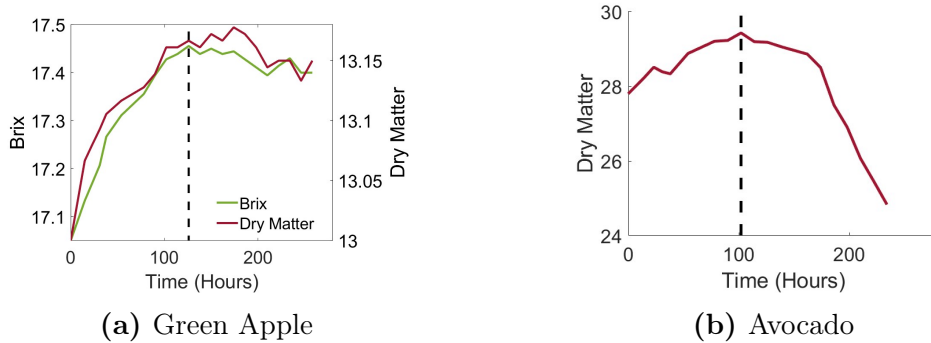


Figure 4.8: Measured Trends in Brix and Dry Matter. The figure shows the Dry Matter values of both the Green Apple and the Avocado in 12-hour intervals over 10 Days



Figure 4.9: This figure shows the PLS Regression results for both Green Apple and Persimmon. x1, x2, x3 represent Red, Green, and Blue respectively. Note that blue (x3) has the lowest P-value for Green Apple but not for Avocado.



Figure 4.10: This figure shows the PLS contribution of the components. In both cases, the first component is the Blue contribution. Hence the intersection with the Y axis represents the contribution of the Blue reflectance.

4.5 Ripeness Metric Estimation Performance and Evaluation

In assessing the performance of the regression models, we calculated the normalized root mean squared errors (RMSE) for the Brix and Dry Matter models in different fruits. The results indicate the following:

- For the Brix model, the normalized RMSE values were 3.05% for Green Apple and 3.37% for Persimmon. These values demonstrate the relatively low prediction errors of the model and its ability to estimate the sugar content accurately, which is crucial for evaluating fruit sweetness and taste.
- The Dry Matter model for Green Apple showed a normalized RMSE value of 0.7%. This indicates the model's effectiveness in predicting the non-water mass percentage in sugary fruits (suggesting Dry Matter is another indication of Brix), an important parameter related to fruit texture and quality.

However, the Dry Matter model for Avocado yielded a relatively weak result with an RMSE value of 2. This indicates a higher prediction error and suggests that the model's performance in estimating the non-water mass of Avocado was not as accurate as in other fruits.

The contrasting performance between avocados and other fruits raises an intriguing question regarding the discrepancy in their regression models. This can be attributed to the functions of pigments within the fruit. Fruits have evolved to establish symbiotic relationships with animals, offering themselves as a food source rich in sugar, while animals contribute to their dispersal by acting as germination vectors [24]. In order to attract animals for consumption, fruits have developed pigments that regulate the ripening process and serve as visual cues [25]. Previous literature supports the notion that fruit color changes can be directly linked to internal sugar concentration [41]. In the case of Avocados, the lack of a high sugar concentration leads to a less pronounced correlation between color reflectance and ripening metrics [31]. Unlike other fruits that undergo significant color changes during ripening due to sugar accumulation, Avocados exhibit shifts in color that may not strongly correspond to changes in ripeness. Therefore, the weaker impact of color on ripening metrics in Avocados can be attributed to their lower sugar content, resulting in a less distinct relationship between color reflectance and ripeness indicators.

In conclusion, the evaluation of the resulting models demonstrates a robust correlation between the sugar content of fruits and the reflectance of colors, specifically in the blue wavelength (430nm). This finding indicates that for climacteric fruits with high sugar content, it is possible to establish ripeness models by implementing a blue mask to directly identify the relationship between color reflectance and ripeness. By focusing on this specific color range, the need for a machine-learning model can be eliminated, allowing for the efficient construction of models without significant bias. This approach offers a practical and expedient solution for fruit ripeness estimation through imaging.

Chapter 5

Discussion and Future Work

5.1 Discussion

The result of this work has many opportunities to be implemented as alluded to earlier in the paper:

- Mobile Applications: With the dimensionality reduction achieved through image sensing, it becomes feasible to implement this technology in low-power IoT devices [53]. This scalability along the supply chain enables the provision of accurate individual measurements at each stage, presenting an opportunity to significantly reduce operating costs.
- Rotting and Decay Sensing: Instead of solely measuring changes until the fruit reaches horticultural maturity, there is potential to develop a model that detects when the fruit reaches senescence by extending the duration of training data collection [8]. By incorporating data from the entire ripening process, a more comprehensive and robust model can be constructed, enhancing the accuracy of rotting and decay sensing.

5.2 Future Work

In order to expand the efficacy of imaging, switching to a hyperspectral imaging system would yield higher bandwidth, allowing for more frequencies to be tested [21]. We can then provide a more accurate wavelength that better corresponds to the sugar concentration than the generalization of Blue at 430 nm.

To further expand on the findings of this project, the developed models can be integrated with other measurement technologies to enhance the overall fruit sensing capabilities. One potential system that can provide scalable non-invasive fruit ripeness metrics is the end-to-end wireless sub-terahertz food sensing system that is currently being developed in the lab the SWAN (Smart Wireless Agile Networks) lab at Princeton, which operates in the wavelength range of 3 mm to $30\text{ }\mu\text{m}$ and is highly sensitive to water.

1. **Imaging (PLSR):** Based on the results obtained in this project, it is evident that the change in blue reflectance is closely correlated with fruit ripeness metrics. Therefore, integrating imaging techniques using a partial least squares (PLS) model can provide accurate measurements of Brix or Dry Matter for fruits with high sugar content.
2. **Sub-Thz Sensing:** Sub-terahertz (Sub-Thz) frequencies, with their penetration ability of up to 0.3mm [4], can enable measurements at both the surface level and beneath the fruit's peel. This may enable ripeness measurement abilities that penetrate within the fruit, providing measurements within the fruits non-invasively. Considering the high absorbance of Sub-Thz frequencies by water [36], this technology can offer precise measurements of Dry Matter. This capability complements the sugar measurement abilities of imaging, particularly for fruits like avocados with minimal sugar content.

By integrating these different approaches, a comprehensive fruit sensing system can be realized, providing accurate and multifaceted assessments of fruit ripeness and quality.

Chapter 6

Conclusion

The results obtained from the imaging techniques showcased in this project validate the feasibility of establishing a direct relationship between blue reflectance and ripeness metrics. This enables our systems to accurately infer the sugar content in fruits, providing a lightweight and bias-resistant approach. As the research progresses, we hope that integrating this with other technologies will yield a more comprehensive and resilient solution, contributing to the sustainability of the food industry and increasing accessibility to fresh food for the global population.

Appendix A

Appendix

A.1 Engineering and Industrial Standards

The independent project described in this thesis incorporated the following engineering and industrial standards:

1. Degrees Brix (Referred to as Brix): Measure of dissolved sugars in fruit in terms of percentage solubility (eg. a Brix of 20 is 20% of sugar dissolved)
2. Dry Matter (DM): Measure of dry mass in a fruit (eg an apple with a DM of 20 is made up of 20% non-water mass).
3. This Independent Project used Matlab to process the data and SI (International System of Units) Units in the creation of the experimental setup.

The following materials have been used:

Item	Quantity
GoPro Hero 10	2
Styrofoam Boards (244 cm by 122 cm)	6
Avocados	10
Persimmon	10
Green Apple	10
Felix F750 Produce Quality Meter	1

A.2 Image Processing

Attached here is the code for the raw GoPro images were broken down and analyzed.

```

1 close all
2 clc
3 %% Settings
4 numFiles = 1:40; %% Number of Files
5 search = 400; %% search region
6 tic
7 debug = false;
8 srgbGen = raw2rgb('TestDay.dng'); %% Generic SRGB
9 srgb = zeros([(length(numFiles))/2, size(srgbGen)], '
10      uint16');
11
12 numLength = length(numFiles)/2; %% half numLength for 12
13      hours
14
15 %% Setting up Parallel Computing Cores Do Not Touch
16 c = parcluster('local');
17 nw = c.NumWorkers ;
18 p = gcp('nocreate');
19 if isempty(p)
20     if (numLength - 1 < nw)
21         parpool(numLength -1)
22     else
23         parpool(nw);
24 end

```

```
24     else
25
26         poolsize = p.NumWorkers;
27
28         if(numlength - 1 > poolsize)
29             delete(gcp('nocreate'));
30
31         if (numlength - 1 < nw)
32             parpool(numlength -1)
33
34         else
35             parpool(nw);
36
37         end
38
39     end
40
41 parfevalOnAll(@warning,0,'off','all');
42
43 %% Persimmon
44
45 %% Load image and pre-allocate matrixes
46 for j = 1:2: length(numFiles) %% every 12 hours
47
48     filename = strcat('2Exp', num2str(numFiles(j)));
49
50     if(isfile(strcat(filename, '.mat')))
51
52         load(strcat(filename, '.mat'))
53
54         srgb(g,:,:, :) = image;
```

```
51    else
52        image = raw2rgb(strcat(filename, '.dng')); %% SRGB File (16 bit)
53        srgb(g,:,:,:)=image;
54        save(strcat(filename, '.mat'), 'image')
55    end
56
57    g = g + 1;
58
59    disp(strcat('2Exp', num2str(numFiles(j)), '.dng'));
60 end
61 fruitValues = zeros([numlength, 10, [201 201 3]], 'uint16');
62 % Array of fruits: experiment number, fruit number
63 image_loc_matrix = zeros(numlength, 10, 4);
64 persimmonDeltaE_matrix = zeros(numlength, 10);
65 persimmonSimilar_matrix = zeros(numlength, 10);
66 max_corr_array = zeros(numlength, 10);
67
68 %% Localize Fruit
69
70 search_loc =[ 2400 2600 2650 2850; ...
71             3700 3900 2600 2800; ...
72             3330 3530 2700 2900; ...
73             2900 3100 2670 2870; ...
74             2400 2600 2670 2870; ...
75             1850 2050 2700 2900; ...
```

```
76      1400 1600 2670 2870; ...
77      900 1100 2670 2870; ...
78      3470 3670 4370 4570; ...
79      3150 3350 4450 4650;
80  ];
81 %% Fruit Positions
82 searchImage = reshape(srgb(1,:,:,:), size(srgbGen));
83 for i = 1:10
84     fruitValues(1, i,:,:,:) = searchImage(search_loc(i,1)
85         :search_loc(i,2),search_loc(i,3):search_loc(i,4)
86         ,:);
87 end
88 tmp = fruitValues;
89 tmp_size = size(searchImage(1500:1700,1900:2100,:));
90 %% Initialize correlation, change time, and errors arrays
91
92
93 parfor k = 1:numlength %% every 12 hours
94     tempImage = reshape(srgb(k,:,:,:), size(srgbGen));
95     tempimagedloc = search_loc;
96     tempimagedloc(:,1) = tempimagedloc(:,1) - search/2;
97     tempimagedloc(:,2) = tempimagedloc(:,2) + search/2;
98     tempimagedloc(:,3) = tempimagedloc(:,3) - search/2;
99     tempimagedloc(:,4) = tempimagedloc(:,4) + search/2;
100
```

```
101 tmpa = tmp;
102
103 original = rgb2gray(searchImage);
104 distorted = rgb2gray(tempImage);
105 tempImage_scaled = rescale(original,distorted,
106                             tempImage);
107
108 disp(strcat('Begin File #', num2str(k)));
109 for i = 1:10
110     ref_img = reshape(tmpa(1, i,:,:,:),[201 201,3]);
111     search_window = tempImage_scaled(tempimagerloc(i
112 ,1):tempimagerloc(i,2),tempimagerloc(i,3):
113 tempimagerloc(i,4),:);
114     ref_img_grey = rgb2gray(reshape(tmpa(1, i,:,:,:)
115 ,[201 201,3]));
116     search_window_grey = rgb2gray(tempImage_scaled(
117 tempimagerloc(i,1):tempimagerloc(i,2),
118 tempimagerloc(i,3):tempimagerloc(i,4),:));
119     c = normxcorr2(ref_img_grey,search_window_grey);
120
121     % offset found by correlation
122     [max_c,imax] = max(abs(c(:)));
123     max_corr_array(k,i) = (max_c);
124     [ypeak,xpeak] = ind2sub(size(c),imax(1));
125     corr_offset = [(xpeak-size(ref_img_grey,2))
126                    (ypeak-size(ref_img_grey,1))];
```

```
122
123     % relative offset of position of subimages
124     rect_offset = [0,0];
125
126
127     % total offset
128     offset = corr_offset + rect_offset;
129     xoffset = offset(1);
130     yoffset = offset(2);
131     image_loc_matrix(k,i,:) = [round(yoffset + 1)
132                                 round(yoffset + size(ref_img_grey,1)) round(
133                                 xoffset + 1) round(xoffset + size(ref_img_grey
134                                 ,2))];
135     image_loc = reshape(image_loc_matrix(k,i,:),[1,4]);
136
137     est_image = search_window(image_loc(1):image_loc
138                               (2), image_loc(3):image_loc(4),:);
139
140     if(debug)
141         figure
142         surf(c)
143         shading flat
144         xbegin = round(xoffset + 1);
145         xend   = round(xoffset + size(ref_img_grey,2)
146                         );
147         ybegin = round(yoffset + 1);
148         yend   = round(yoffset + size(ref_img_grey,1)
149                         );
```

```
142
143     recovered_img = uint16(zeros(size(
144         search_window)));
144     recovered_img(ybegin:yend, xbegin:xend, :) =
145         ref_img;
145
146 %         figure
147 %             imshowpair(rgb2gray(search_window),
148 %                         recovered_img, "blend")
148 %
149 %         figure
150 %             imshow(search_window)
150
151 %% delta e (can we see it)
152 persimmonDeltaE_matrix(k,i) = mean(imcolordiff(
153     ref_img, est_image), 'all');
153
154 %% color components
155 persimmonRedSsim(k,i) = ssim(ref_img(:,:,1),
156     est_image(:,:,1));
156 persimmonGreenSsim(k,i) = ssim(ref_img(:,:,2),
157     est_image(:,:,2));
157 persimmonBlueSsim(k,i) = ssim(ref_img(:,:,3),
158     est_image(:,:,3));
158
159 %% energies
```

```
161     persimmonSimilar_matrix(k,i) = ssim(ref_img_grey,
162                                         rgb2gray(est_image));
163
164
165
166 end
167
168
169
170
171 %% Calculates Median Delta E and SSIM
172 persimmonDeltaE = smooth(median(persimmonDeltaE_matrix,2),
173                           , 10);
173 persimmonSsimval = smooth(median(persimmonSimilar_matrix
174                           ,2), 10);
174 median_similarity = smooth(median(persimmonSimilar_matrix
175                           ,2), 10);
175 median_deltaE = smooth(median(persimmonDeltaE_matrix,2),
176                           , 10);
176 save('Persimmon_Similarity_DeltaE.mat','
177       persimmonDeltaE_matrix','persimmonSimilar_matrix','
178       median_similarity','median_deltaE')
177 %% Plot greenAppledeltaE and SSIM
178 figure
179 plot(2:numlength,persimmonDeltaE(2:numlength),'-o',
180       'Linewidth',4)
```

```
180 hold off
181 ax = gca;
182 ax.FontSize = 30;
183 title("Persimmon à E Values in Relation to First
        Experiment (Experiment Pictures, excluding first data
        point)")
184 xlabel('Experiment Number (Every 12 hours)')
185 ylabel('à E compared to 1st Day')
186 legend('show')
187 box off
188
189 figure
190 plot(2:numlength,persimmonSsimval(2:numlength), '-o', '
        Linewidth',4)
191 hold off
192 ax = gca;
193 ax.FontSize = 30;
194 title("Persimmon SSIM Values in Relation to First
        Experiment (Experiment Pictures, excluding first data
        point)")
195 xlabel('Experiment Number (Every 12 hours)')
196 ylabel('SSIM compared to 1st Day')
197 legend('show')
198 box off
199 ylim([0 1])
200
201 PRssimval = smooth(median(persimmonRedSsim,2), 10);
```

```

202 PGssimval = smooth(median(persimmonGreenSsim,2), 10);
203 PBssimval = smooth(median(persimmonBlueSsim,2), 10);
204
205
206 %% Green Apple
207
208
209
210 %%%%%% GREEN APPLE AND AVOCADO %%%%%%
211
212
213 g=1;
214
215 %%% Avocado
216
217 %% Load image and pre-allocate matrixes
218 for j = 1:2: length(numFiles) %% every 12 hours
219     filename = strcat('1Exp', num2str(numFiles(j)));
220     if(isfile(strcat(filename, '.mat')))
221         load(strcat(filename, '.mat'))
222         srgb(g,:,:, :) = image;
223     else
224         image = raw2rgb(strcat(filename, '.dng')); %%
225             SRGB File (16 bit)
226         srgb(g,:,:, :) = image;
227         save(strcat(filename, '.mat'), 'image')
228     end

```

```
228
229     g = g + 1;
230
231     disp(strcat('1Exp', num2str(numFiles(j)), '.dng'));
232 end
233 fruitValues = zeros([numlength, 10, [201 201 3]], 'uint16'
234     ); % Array of fruits: experiment number, fruit number
235 image_loc_matrix = zeros(numlength, 10, 4);
236 avocadoDeltaE_matrix = zeros(numlength, 10);
237 avocadoSimilar_matrix = zeros(numlength, 10);
238 max_corr_array = zeros(numlength, 10);
239
240 %% Localize Fruit
241
242 search_loc =[ 270 470 4000 4200; ...
243                 630 830 4000 4200; ...
244                 1100 1300 4100 4300; ...
245                 1500 1700 4150 4350; ...
246                 1950 2150 4200 4400; ...
247                 2400 2600 4200 4400; ...
248                 2850 3050 4120 4320; ...
249                 201 401 2000 2200; ...
250                 600 800 1950 2150; ...
251                 1000 1200 1950 2150;
252 ];
253 %% Fruit Positions
```

```
254 searchImage = reshape(srgb(1,:,:,:,:), size(srgbGen));  
255 for i = 1:10  
256     fruitValues(1, i,:,:,:) = searchImage(search_loc(i,1)  
257         :search_loc(i,2),search_loc(i,3):search_loc(i,4)  
258         ,:);  
259 end  
260 tmp = fruitValues;  
261 tmp_size = size(searchImage(1500:1700,1900:2100,:));  
262 %% Initialize correlation, change time, and errors arrays  
263  
264  
265 parfor k = 1:numlength  
266     tempImage = reshape(srgb(k,:,:,:,:), size(srgbGen));  
267     tempimagedloc = search_loc;  
268     tempimagedloc(:,1) = tempimagedloc(:,1) - search/2;  
269     tempimagedloc(:,2) = tempimagedloc(:,2) + search/2;  
270     tempimagedloc(:,3) = tempimagedloc(:,3) - search/2;  
271     tempimagedloc(:,4) = tempimagedloc(:,4) + search/2;  
272  
273     tmpa = tmp;  
274  
275     original = rgb2gray(searchImage);  
276     distorted = rgb2gray(tempImage);  
277     tempImage_scaled = rescale(original,distorted,  
278         tempImage);
```

```
278
279
280 disp(strcat('Begin File #', num2str(k)));
281 for i = 1:10
282     ref_img = reshape(tmpa(1, i,:,:,:), [201 201,3]);
283     search_window = tempImage_scaled(tempimagedoc(i
284         ,1):tempimagedoc(i,2),tempimagedoc(i,3):
285         tempimagedoc(i,4),:);
286     ref_img_grey = rgb2gray(reshape(tmpa(1, i,:,:,:)
287         ,[201 201,3]));
288     search_window_grey = rgb2gray(tempImage_scaled(
289         tempimagedoc(i,1):tempimagedoc(i,2),
290         tempimagedoc(i,3):tempimagedoc(i,4),:));
291     c = normxcorr2(ref_img_grey,search_window_grey);
292
293
294     % offset found by correlation
295     [max_c,imax] = max(abs(c(:)));
296     max_corr_array(k,i) = (max_c);
297     [ypeak,xpeak] = ind2sub(size(c),imax(1));
298     corr_offset = [(xpeak-size(ref_img_grey,2))
299                     (ypeak-size(ref_img_grey,1))];
299
300
301     % relative offset of position of subimages
302     rect_offset = [0,0];
303
304
305     % total offset
```

```
300     offset = corr_offset + rect_offset;
301
302     xoffset = offset(1);
303
304     yoffset = offset(2);
305
306     image_loc_matrix(k,i,:) = [round(yoffset + 1)
307                               round(yoffset + size(ref_img_grey,1)) round(
308                               xoffset + 1) round(xoffset + size(ref_img_grey
309                               ,2))];
310
311     image_loc = reshape(image_loc_matrix(k,i,:),[1,4]);
312
313
314
315
316     if image_loc(2) > 601
317         image_loc(1) = 401;
318
319         image_loc(2) = 601;
320
321         end
322
323
324
325
326     if image_loc(4) > 601
327         image_loc(3) = 401;
328
329         image_loc(4) = 601;
330
331         end
332
333
334
335
336     if image_loc(3) < 0
337         image_loc(3) = 1;
338
339         image_loc(4) = 201;
```

```
323     end
324
325
326     est_image = search_window(image_loc(1):image_loc
327                               (2), image_loc(3):image_loc(4), :);
327 if(debug)
328     figure
329     surf(c)
330     shading flat
331     xbegin = round(xoffset + 1);
332     xend   = round(xoffset + size(ref_img_grey,2)
333                   );
334     ybegin = round(yoffset + 1);
335     yend   = round(yoffset + size(ref_img_grey,1)
336                   );
336
336     recovered_img = uint16(zeros(size(
337                                   search_window)));
337     recovered_img(ybegin:yend,xbegin:xend,:) =
338         ref_img;
338     imshowpair(rgb2gray(search_window),
339                 recovered_img,"blend")
339 %             figure
340 %             imshowpair(rgb2gray(est_image),ref_img,
340 % "blend")
341 %             figure
342 %             imshow(search_window)
```

```
343     end
344
345     avocadoDeltaE_matrix(k,i) = mean(imcolordiff(
346         ref_img,est_image), 'all');
347 %% Split into colors
348 avocadoRedSsim(k,i) = ssim(ref_img(:,:,1),est_image
349     (:,:,1));
350         avocadoGreenSsim(k,i) = ssim(ref_img(:,:,2),
351             est_image(:,:,2));
352         avocadoBlueSsim(k,i) = ssim(ref_img(:,:,3),
353             est_image(:,:,3));
354
355
356     avocadoSimilar_matrix(k,i) = ssim(ref_img_grey,
357         rgb2gray(est_image));
358
359
360     end
361
362
363
364 end
```

```
365 %% Calculates Median Delta E and SSIM
366
367 ARssimval = smooth(median(avocadoRedSsim,2), 10);
368 AGssimval = smooth(median(avocadoGreenSsim,2), 10);
369 ABssimval = smooth(median(avocadoBlueSsim,2), 10);
370
371
372
373 avocadoDeltaE = smooth(median(avocadoDeltaE_matrix,2),
374 10);
374 avocadoSsimval = smooth(median(avocadoSimilar_matrix,2),
375 10);
375 median_similarity = smooth(median(avocadoSimilar_matrix
376 ,2), 10);
376 median_deltaE = smooth(median(avocadoDeltaE_matrix,2),
377 10);
377 save('Avacodo_Similarity_DeltaE.mat','avocadoDeltaE_matrix
378 ','avocadoSimilar_matrix','median_similarity','
379 median_deltaE')
380 %% Plot DeltaE and SSIM
381 figure
382 plot(2:numlength,avocadoDeltaE(2:numlength),'-o',
383 'LineWidth',4)
384 hold off
385 ax = gca;
386 ax.FontSize = 30;
387 title("Avocado à E Values in Relation to First
```

```
    Experiment (Experiment Pictures, excluding first data
    point)")

385 xlabel('Experiment Number (Every 12 hours)')
386 ylabel('SSIM compared to 1st Day')
387 legend('show')
388 box off
389
390 figure
391 plot(2:numlength,avocadoSsimval(2:numlength),'-o','
        Linewidth',4)
392 hold off
393 ax = gca;
394 ax.FontSize = 30;
395 title("Avacodo SSIM Values in Relation to First
        Experiment (Experiment Pictures, excluding first data
        point)")

396 xlabel('Experiment Number (Every 12 hours)')
397 ylabel('SSIM compared to 1st Day')
398 legend('show')
399 box off
400 ylim([0 1])
401
402
403
404
405
406 fruitValues = zeros([numlength, 10, [201 201 3]],'uint16'
```

```

); %% Array of fruits: experiment number, fruit number

407 image_loc_matrix = zeros(numlength,10,4);
408 greenAppleDeltaE_matrix = zeros(numlength,10);
409 greenAppleSimilar_matrix = zeros(numlength,10);
410 max_corr_array = zeros(numlength,10);

411
412

413 %% Localize Fruit

414

415 search_loc =[ 1500 1700 1900 2100; ...
416
417     1950 2150 1900 2100; ...
418     2500 2700 1900 2100; ...
419     2920 3120 1900 2100; ...
420     510   710   550   750; ...
421     900   1100  430   630; ...
422     1220  1420  430   630; ...
423     1550  1750  430   630; ...
424     2000  2200  350   550; ...
425     2350  2550  400   600;
426 ];
427
428 %% Fruit Positions
429
430 for i = 1:10
431
432     fruitValues(1, i,:,:,:) = searchImage(search_loc(i,1)
433
434         :search_loc(i,2),search_loc(i,3):search_loc(i,4)
435
436         ,:);
437
438 end

```

```
431 tmp = fruitValues;
432 tmp_size = size(searchImage(1500:1700,1900:2100,:));
433 %% Initialize correlation, change time, and errors arrays
434
435
436
437 parfor k = 1:numlength
438     tempImage = reshape(srgb(k,:,:,:,1), size(srgbGen));
439     tempimagedoc = search_loc;
440     tempimagedoc(:,1) = tempimagedoc(:,1) - search/2;
441     tempimagedoc(:,2) = tempimagedoc(:,2) + search/2;
442     tempimagedoc(:,3) = tempimagedoc(:,3) - search/2;
443     tempimagedoc(:,4) = tempimagedoc(:,4) + search/2;
444
445     tmpa = tmp;
446
447     original = rgb2gray(searchImage);
448     distorted = rgb2gray(tempImage);
449     tempImage_scaled = rescale(original,distorted,
450                               tempImage);
451
452     disp(strcat('Begin File #', num2str(k)));
453     for i = 1:10
454         ref_img = reshape(tmpa(1, i,:,:,:,1), [201 201,3]);
455         search_window = tempImage_scaled(tempimagedoc(i
456 ,1):tempimagedoc(i,2),tempimagedoc(i,3):
```

```
        tempimageloc(i,4),:);  
456 ref_img_grey = rgb2gray(reshape(tmpa(1, i,:,:,:,:,  
        ,[201 201,3]));  
457 search_window_grey = rgb2gray(tempImage_scaled(  
        tempimageloc(i,1):tempimageloc(i,2),  
        tempimageloc(i,3):tempimageloc(i,4),:));  
458 c = normxcorr2(ref_img_grey,search_window_grey);  
459  
460 % offset found by correlation  
461 [max_c,imax] = max(abs(c(:)));  
462 max_corr_array(k,i) = (max_c);  
463 [ypeak,xpeak] = ind2sub(size(c),imax(1));  
464 corr_offset = [(xpeak-size(ref_img_grey,2))  
465             (ypeak-size(ref_img_grey,1))];  
466  
467 % relative offset of position of subimages  
468 rect_offset = [0,0];  
469  
470  
471 % total offset  
472 offset = corr_offset + rect_offset;  
473 xoffset = offset(1);  
474 yoffset = offset(2);  
475 image_loc_matrix(k,i,:) = [round(yoffset + 1)  
        round(yoffset + size(ref_img_grey,1)) round(  
        xoffset + 1) round(xoffset + size(ref_img_grey  
        ,2))];
```

```
476     image_loc = reshape(image_loc_matrix(k,i,:),
477                           [1,4]);
478
479     est_image = search_window(image_loc(1):image_loc
480                               (2), image_loc(3):image_loc(4),:);
481
482     if(debug)
483
484         figure
485
486         surf(c)
487
488         shading flat
489
490         xbegin = round(xoffset + 1);
491
492         xend = round(xoffset + size(ref_img_grey,2)
493
494             );
495
496         ybegin = round(yoffset + 1);
497
498         yend = round(yoffset + size(ref_img_grey,1)
499
500             );
501
502
503         recovered_img = uint16(zeros(size(
504
505             search_window)));
506
507         recovered_img(ybegin:yend,xbegin:xend,:) =
508
509             ref_img;
510
511         imshowpair(rgb2gray(search_window),
512
513             recovered_img,"blend")
514
515         %
516         %         figure
517         %
518         %         imshowpair(rgb2gray(est_image),ref_img,
519
520             "blend")
521
522         %
523         %         figure
524         %
525         %         imshow(search_window)
526
527     end
```

```
495 greenAppleRedSsim(k,i) = ssim(ref_img(:,:,1),  
496 est_image(:,:,1));  
496 greenAppleGreenSsim(k,i) = ssim(ref_img  
497(:,:,2),est_image(:,:,2));  
497 greenAppleBlueSsim(k,i) = ssim(ref_img(:,:,3)  
498 ,est_image(:,:,3));  
498 greenAppleDeltaE_matrix(k,i) = mean(imcolordiff(  
499 ref_img,est_image),'all');  
499 greenAppleSimilar_matrix(k,i) = ssim(ref_img_grey  
500 ,rgb2gray(est_image));  
500 end  
501 disp(strcat('File #', num2str(k), ' completed!'));  
502  
503  
504 end  
505  
506  
507  
508  
509 %% Calculates Median Delta E and SSIM  
510 greenAppleDeltaE = smooth(median(greenAppleDeltaE_matrix  
511 ,2), 10);  
511 greenAppleSsimval = smooth(median(  
512 greenAppleSimilar_matrix,2), 10);  
512 median_similarity = smooth(median(  
513 greenAppleSimilar_matrix,2), 10);  
513 median_deltaE = smooth(median(greenAppleDeltaE_matrix,2),
```

```
    10);

514 GRssimval = smooth(median(greenAppleRedSsim,2), 10);
515 GGssimval = smooth(median(greenAppleGreenSsim,2), 10);
516 GBssimval = smooth(median(greenAppleBlueSsim,2), 10);
517
518
519
520 save('GreenApple_Similarity_DeltaE.mat',
521       'greenAppleDeltaE_matrix','greenAppleSimilar_matrix',
522       'median_similarity','median_deltaE')

523 %% Plot DeltaE and SSIM
524 figure
525 plot(2:numlength,greenAppleDeltaE(2:numlength), '-o',
526       'LineWidth',4)
527 hold off
528 ax = gca;
529 ax.FontSize = 30;
530 title("Green Apple à E Values in Relation to First
531        Experiment (Experiment Pictures, excluding first data
532        point)")
533 xlabel('Experiment Number (Every 12 hours)')
534 ylabel('à E compared to 1st Day')
535 legend('show')
536 box off
537
538 figure
539 plot(2:numlength,greenAppleSsimval(2:numlength), '-o',
540       'LineWidth',4)
```

```
    'Linewidth',4)

535 hold off
536 ax = gca;
537 ax.FontSize = 30;
538 title("Green Apple SSIM Values in Relation to First
      Experiment (Experiment Pictures, excluding first data
      point)")

539 xlabel('Experiment Number (Every 12 hours)')
540 ylabel('SSIM compared to 1st Day')
541 legend('show')
542 box off

543
544
545 %% Plot all SSIM in single graph
546
547
548 figure('Renderer', 'painters', 'Position', [100 100 9000
      6000])
549 plot(2:numlength,greenAppleSsimval(2:numlength), '-o',
      'Linewidth',4)
550 hold on
551 plot(2:numlength,avocadoSsimval(2:numlength), '-square',
      'Linewidth',4)
552 hold on
553 plot(2:numlength,persimmonSsimval(2:numlength), '-diamond'
      , 'Linewidth',4)
554 ylim([0.4 1])
```

```
555
556
557 hold off
558 ax = gca;
559 ax.FontSize = 30;
560 title("Fruit SSIM Values in Relation to First Experiment
      (Experiment Pictures, excluding first data point)")
561 xlabel('Experiment Number (Every 12 hours)')
562 ylabel('SSIM compared to 1st Day')
563 legend('Green Apple', 'Avocado', 'Persimmon')
564 box off
565
566
567 %% Plot Delta E in a graph
568
569 figure('Renderer', 'painters', 'Position', [100 100 9000
      6000])
570
571 plot(2:numlength,greenAppleDeltaE(2:numlength), '-o',
      'Linewidth', 4)
572 hold on
573 plot(2:numlength,avocadoDeltaE(2:numlength), '-square',
      'Linewidth', 4)
574 hold on
575 plot(2:numlength,persimmonDeltaE(2:numlength), '-o',
      'Linewidth', 4)
576
```

```
577
578 hold off
579 ax = gca;
580 ax.FontSize = 30;
581 title("Fruit Delta E Values in Relation to First
      Experiment (Experiment Pictures, excluding first data
      point)")
582 xlabel('Experiment Number (Every 12 hours)')
583 ylabel('SSIM compared to 1st Day')
584 legend('Green Apple', 'Avocado', 'Persimmon')
585 box off
586
587
588 %% Brix Correlation GA
589 GAFelix = table2array(readtable('GAFelix.xlsx','Format',
      'auto'));
590
591
592 GAindVar = [GRssimval, GGssimval, GBssimval];
593 GAdepVar = smooth(median(GAFelix,2), 10);
594
595 fitlm(GAindVar,GAdepVar)
596 [XL,yl,XS,YS,beta,PCTVAR] = plsregress (GAindVar,GAdepVar
      ,3)
597 plot(1:3,cumsum(100*PCTVAR(2,:)), '-bo');
598 xlabel('Number of PLS components in Green Apple');
599 ylabel('Percent Variance Explained in Brix');
```

```
600
601 title("Partial Least Squares Regression Components in
602     Green Apple");
603
604 hold off
605 ax = gca;
606 ax.FontSize = 30;
607 box off
608
609 %% DM Correlation GA
610
611
612 GADMFelix = table2array(readtable('FelixGADM.xlsx',
613     Format,'auto'));
614
615
616 GADMindVar = [GRssimval, GGssimval, GBssimval];
617 GADMdepVar = smooth(median(GADMFelix,2), 10);
618
619 fitlm(GADMindVar,GADMdepVar)
620 [XL,yl,XS,YS,beta,PCTVAR] = plsregress (GADMindVar,
621     GADMdepVar,3)
622 plot(1:3,cumsum(100*PCTVAR(2,:)), '-bo');
623 xlabel('Number of PLS components in Green Apple');
624 ylabel('Percent Variance Explained in DM');
```

```
624 title("Partial Least Squares Regression Components in  
625     Green Apple");  
626  
627 hold off  
628 ax = gca;  
629 ax.FontSize = 30;  
630 box off  
631  
632  
633 %% DM Correlation AV  
634  
635 AVFelix = table2array(readtable('AVDry.xlsx','Format','  
636     auto'));  
637 AVindVar = [ARssimval, AGssimval, ABssimval];  
638 AVdepVar = smooth(median(AVFelix,2), 10);  
639 fitlm(AVindVar,AVdepVar)  
640 [XL,yl,XS,YS,beta,PCTVAR] = plsregress (AVindVar,AVdepVar  
641     ,3)  
642 plot(1:3,cumsum(100*PCTVAR(2,:)), '-bo');  
643 xlabel('Number of PLS components in Avocado');  
644 ylabel('Percent Variance Explained in DM');  
645  
646 title("Partial Least Squares Regression Components in  
Avocado");  
647
```

```
647
648
649 hold off
650 ax = gca;
651 ax.FontSize = 30;
652 box off
653
654
655
656 %% Brix Correlation PE
657
658 peFelix = table2array(readtable('PEFelix.xlsx','Format','
659 auto'));
660 felixPe = smooth(median(peFelix,2), 10);
661
662
663 %%https://www.researchgate.net/post/How\_can\_I\_determine\_the\_relative\_contribution\_of\_predictors\_in\_multiple\_regression
664
665 indVar = [PRssimval, PGssimval, PBssimval];
666 depVar = felixPe;
667 fitlm(indVar,depVar)
668 [XL,YL,XS,YS,BETA,PCTVAR,MSE,stats] = plsregress (indVar,
669 depVar,3)
```

```
670
671
672 figure('Renderer', 'painters', 'Position', [100 100 9000
6000])
673
674 plot(1:3, cumsum(100*PCTVAR(2,:)), '-bo');
675 xlabel('Number of PLS components in Perssimon');
676 ylabel('Percent Variance Explained in Brix');
677
678 title("Partial Least Squares Regression Components in
Perssimon");
679
680
681
682
683 hold off
684 ax = gca;
685 ax.FontSize = 30;
686 box off
687
688
689 %% Green Apple Color Components
690
691
692 figure('Renderer', 'painters', 'Position', [10 10 900
600])
693
```

```
694
695 plot(2:numlength,greenAppleSSimval(2:numlength), '-diamond'
       , 'Linewidth', 4, 'color', 'black')
696 hold on
697 plot(2:numlength,GBSSimval(2:numlength), '-square', '
       Linewidth', 4, 'color', 'blue')
698 hold on
699 plot(2:numlength,GRSSimval(2:numlength), '-o', 'Linewidth'
       , 4, 'color', 'red')
700 hold on
701 plot(2:numlength,GGSSimval(2:numlength), '-*', 'Linewidth'
       , 4, 'color', 'green')
702 hold off
703 ax = gca;
704 ax.FontSize = 30;
705 title("Green Apple SSIM Values in Relation to First
         Experiment (Experiment Pictures, excluding first data
         point)")
706 xlabel('Experiment Number (Every 12 hours)')
707 ylabel('SSIM compared to 1st Day')
708 legend('Grey Scale', 'Blue', 'Red', 'Green')
709 box off
710
711 %% Persimmon Color Components
712 figure('Renderer', 'painters', 'Position', [100 100 9000
       6000])
713
```

```
714 plot(2:numlength,persimmonSSimval(2:numlength),'-diamond'
      , 'Linewidth',4, 'color', 'black')
715 hold on
716 plot(2:numlength,PBssimval(2:numlength),'-square',
      'Linewidth',4, 'color', 'blue')
717 hold on
718 plot(2:numlength,PRssimval(2:numlength),'-o','Linewidth'
      ,4, 'color', 'red')
719 hold on
720 plot(2:numlength,PGssimval(2:numlength),'-*','Linewidth'
      ,4, 'color', 'green')
721 title("Persimmon SSIM Values in Relation to First
          Experiment (Experiment Pictures, excluding first data
          point)")
722 xlabel('Experiment Number (Every 12 hours)')
723 ylabel('SSIM compared to 1st Day')
724 legend('Grey Scale', 'Blue', 'Red', 'Green')
725
726
727 ylim([0.4 1])
728 hold off
729 ax = gca;
730 ax.FontSize = 30;
731 box off
732
733 toc
734
```

```
735 %% Helper Function
736 function image_recover = rescale(original,distorted,
737 tempImage)
738 ptsOriginal = detectSURFFeatures(original);
739 ptsDistorted = detectSURFFeatures(distorted);
740 [featuresOriginal,validPtsOriginal] = extractFeatures
741 (original,ptsOriginal);
742 [featuresDistorted,validPtsDistorted] =
743 extractFeatures(distorted,ptsDistorted);
744 indexPairs = matchFeatures(featuresOriginal,
745 featuresDistorted);
746 matchedOriginal = validPtsOriginal(indexPairs(:,1));
747 matchedDistorted = validPtsDistorted(indexPairs(:,2))
748 ;
749 [tform, inlierIdx] = estgeotform2d(matchedDistorted,
750 matchedOriginal,'similarity');
751 inlierDistorted = matchedDistorted(inlierIdx,:);
752 inlierOriginal = matchedOriginal(inlierIdx,:);
753 invTform = invert(tform);
754 Ainv = invTform.A;
755
756 ss = Ainv(1,2);
757 sc = Ainv(1,1);
758 scaleRecovered = hypot(ss,sc);
759 disp(['Recovered scale: ', num2str(scaleRecovered)])
760
761 % Recover the rotation in which a positive value
```

```
represents a rotation in  
756 % the clockwise direction.  
757 thetaRecovered = atan2d(-ss,sc);  
758 disp(['Recovered theta: ', num2str(thetaRecovered)]);  
759 outputView = imref2d(size(original));  
760 image_recover = imwarp(tempImage,tform,OutputView=  
    outputView);  
761 end
```

Bibliography

- [1] F750 felix produce meter product page, url: <https://felixinstruments.com/food-science-instruments/nir-spectroscopy/f-750-produce-quality-meter/>. Accessed: 2023-5-9.
- [2] Food loss and questions about the amount and causes still remain, url: <https://www.feedingamerica.org/our-work/reduce-food-waste>, 2014. Accessed: 2023-03-11.
- [3] Food waste and food rescue, url: <https://www.feedingamerica.org/our-work/reduce-food-waste>, 2023. Accessed: 2023-03-11.
- [4] A. Abbaszadeh, M. Ahmadi-Boroujeni, and A. Tehranian. A compact polarization insensitive all-dielectric metasurface lens for gaussian to tophat beam shaping in sub-terahertz regime. *Optics Communications*, 462:125313, 2020.
- [5] I. Bakurov, M. Buzzelli, R. Schettini, M. Castelli, and L. Vanneschi. Structural similarity index (ssim) revisited: A data-driven approach. *Expert Systems with Applications*, 189:116087, 2022.
- [6] P. Baldi and P. Sadowski. The dropout learning algorithm. *Artificial intelligence*, 210:78–122, 2014.
- [7] A. Brodziak, J. Król, A. Matwijczuk, T. Czernecki, P. Glibowski, Ł. Wlazło,

- and A. Litwińczuk. Effect of sea buckthorn (*hippophae rhamnoides* l.) mousse on properties of probiotic yoghurt. *Applied Sciences*, 11(2):545, 2021.
- [8] D. A. Brummell, V. Dal Cin, C. H. Crisosto, and J. M. Labavitch. Cell wall metabolism during maturation, ripening and senescence of peach fruit. *Journal of experimental botany*, 55(405):2029–2039, 2004.
- [9] W. Castro, J. Oblitas, M. De-La-Torre, C. Cotrina, K. Bazán, and H. Avila-George. Classification of cape gooseberry fruit according to its level of ripeness using machine learning techniques and different color spaces. *IEEE access*, 7:27389–27400, 2019.
- [10] P. Castro-Valdecantos, O. Apolo-Apolo, M. Pérez-Ruiz, and G. Egea. Leaf area index estimations by deep learning models using rgb images and data fusion in maize. *Precision Agriculture*, 23(6):1949–1966, 2022.
- [11] K. S. Chia, M. N. H. Jam, Z. Gan, and N. Ismail. Pre-dispersive near-infrared light sensing in non-destructively classifying the brix of intact pineapples. *Journal of Food Science and Technology*, 57:4533–4540, 2020.
- [12] K. A. Cox, T. K. McGhie, A. White, and A. B. Woolf. Skin colour and pigment changes during ripening of âhassâ avocado fruit. *Postharvest Biology and Technology*, 31(3):287–294, 2004.
- [13] V. M. Dembitsky, S. Poovarodom, H. Leontowicz, M. Leontowicz, S. Vearasilp, S. Trakhtenberg, and S. Gorinstein. The multiple nutrition properties of some exotic fruits: Biological activity and active metabolites. *Food research international*, 44(7):1671–1701, 2011.
- [14] N. El-Bendary, E. El Hariri, A. E. Hassanien, and A. Badr. Using machine learning techniques for evaluating tomato ripeness. *Expert Systems with Applications*, 42(4):1892–1905, 2015.

- [15] M. Esteki, Z. Shahsavari, and J. Simal-Gandara. Food identification by high performance liquid chromatography fingerprinting and mathematical processing. *Food Research International*, 122:303–317, 2019.
- [16] T. L. Fess, J. B. Kotcon, and V. A. Benedito. Crop breeding for low input agriculture: a sustainable response to feed a growing world population. *Sustainability*, 3(10):1742–1772, 2011.
- [17] J. Gamble, F. R. Harker, S. R. Jaeger, A. White, C. Bava, M. Beresford, B. Stubbings, M. Wohlers, P. J. Hofman, R. Marques, et al. The impact of dry matter, ripeness and internal defects on consumer perceptions of avocado quality and intentions to purchase. *Postharvest Biology and Technology*, 57(1):35–43, 2010.
- [18] V. Giovenzana, R. Beghi, A. Mena, and R. Civelli. Section 4 quick quality evaluation of chilean grapes by a portable vis/nir device. *Application of vis/NIR spectroscopy for ripeness evaluation and postharvest quality analysis of agro-food products*, page 135, 2012.
- [19] S. Goisser, S. Wittmann, and H. Mempel. Food-scanner applications in the fruit and vegetable sector. *Landtechnik*, 76(1), 2021.
- [20] B. Gong, Y. Shi, F. Sha, and K. Grauman. Geodesic flow kernel for unsupervised domain adaptation. In *2012 IEEE conference on computer vision and pattern recognition*, pages 2066–2073. IEEE, 2012.
- [21] C. Guo, F. Liu, W. Kong, Y. He, B. Lou, et al. Hyperspectral imaging analysis for ripeness evaluation of strawberry with support vector machine. *Journal of Food Engineering*, 179:11–18, 2016.
- [22] S. Gutiérrez, A. Wendel, and J. Underwood. Spectral filter design based on in-

- field hyperspectral imaging and machine learning for mango ripeness estimation. *Computers and Electronics in Agriculture*, 164:104890, 2019.
- [23] G. Guven and H. Samkar. Examination of dimension reduction performances of plsr and pcr techniques in data with multicollinearity. *Iranian Journal of Science and Technology, Transactions A: Science*, 43:969–978, 2019.
- [24] C. M. Herrera. Seed dispersal by vertebrates. *Plant–animal interactions: an evolutionary approach*, pages 185–208, 2002.
- [25] L. Kapoor, A. J. Simkin, C. George Priya Doss, and R. Siva. Fruit ripening: dynamics and integrated analysis of carotenoids and anthocyanins. *BMC plant biology*, 22(1):1–22, 2022.
- [26] H. Kaur, R. Künnemeyer, and A. McGlone. Comparison of hand-held near infrared spectrophotometers for fruit dry matter assessment. *Journal of Near Infrared Spectroscopy*, 25(4):267–277, 2017.
- [27] N. Khamis, H. Selamat, S. Ghazalli, N. I. M. Saleh, and N. Yusoff. Comparison of palm oil fresh fruit bunches (ffb) ripeness classification technique using deep learning method. In *2022 13th Asian Control Conference (ASCC)*, pages 64–68. IEEE, 2022.
- [28] L. Kitinoja, S. Saran, S. K. Roy, and A. A. Kader. Postharvest technology for developing countries: challenges and opportunities in research, outreach and advocacy. *Journal of the Science of Food and Agriculture*, 91(4):597–603, 2011.
- [29] E. Kress-Rogers and C. J. Brimelow. *Instrumentation and sensors for the food industry*, volume 65. Woodhead Publishing, 2001.
- [30] H. Lee and G. Coates. Quantitative study of free sugars and myo-inositol in citrus juices by hplc and a literature compilation. 2000.

- [31] S.-K. Lee. A review and background of the avocado maturity standard. *California Avocado Society Yearbook*, 65:101–109, 1981.
- [32] M. Lindley. The impact of food processing on antioxidants in vegetable oils, fruits and vegetables. *Trends in Food Science & Technology*, 9(8-9):336–340, 1998.
- [33] N. Mehrabi, F. Morstatter, N. Saxena, K. Lerman, and A. Galstyan. A survey on bias and fairness in machine learning. *ACM Computing Surveys (CSUR)*, 54(6):1–35, 2021.
- [34] A. Muller, C. Schader, N. El-Hage Scialabba, J. Brüggemann, A. Isensee, K.-H. Erb, P. Smith, P. Klocke, F. Leiber, M. Stolze, et al. Strategies for feeding the world more sustainably with organic agriculture. *Nature communications*, 8(1):1–13, 2017.
- [35] M. Oren-Shamir. Does anthocyanin degradation play a significant role in determining pigment concentration in plants? *Plant Science*, 177(4):310–316, 2009.
- [36] Y. Oyama, L. Zhen, T. Tanabe, and M. Kagaya. Sub-terahertz imaging of defects in building blocks. *Ndt & E International*, 42(1):28–33, 2009.
- [37] J. W. Palmer, F. R. Harker, D. S. Tustin, and J. Johnston. Fruit dry matter concentration: a new quality metric for apples. *Journal of the Science of Food and Agriculture*, 90(15):2586–2594, 2010.
- [38] A. Payasi and G. Sanwal. Ripening of climacteric fruits and their control. *Journal of food Biochemistry*, 34(4):679–710, 2010.
- [39] L. Pereira, M. Pujol, J. Garcia-Mas, and M. A. Phillips. Non-invasive quantification of ethylene in attached fruit headspace at 1 ppb by gas chromatography–mass spectrometry. *The Plant Journal*, 91(1):172–183, 2017.

- [40] V. Prasanna, T. Prabha, and R. Tharanathan. Fruit ripening phenomena—an overview. *Critical reviews in food science and nutrition*, 47(1):1–19, 2007.
- [41] P. Riba-Hernández, K. E. Stoner, and P. W. Lucas. Sugar concentration of fruits and their detection via color in the central american spider monkey (*ateles geoffroyi*). *American Journal of Primatology: Official Journal of the American Society of Primatologists*, 67(4):411–423, 2005.
- [42] A. Rodríguez, B. Alquézar, and L. Peña. Fruit aromas in mature fleshy fruits as signals of readiness for predation and seed dispersal. *New Phytologist*, 197(1):36–48, 2013.
- [43] D. Ruiz and J. Egea. Phenotypic diversity and relationships of fruit quality traits in apricot (*prunus armeniaca l.*) germplasm. *Euphytica*, 163:143–158, 2008.
- [44] Ruvi. Will the drought cause a shortage in fruits amp; veggies?
- [45] I. A. Sabilla, C. S. Wahyuni, C. Faticahah, and D. Herumurti. Determining banana types and ripeness from image using machine learning methods. In *2019 International Conference of Artificial Intelligence and Information Technology (ICAIIT)*, pages 407–412. IEEE, 2019.
- [46] E. Sanchís, S. Gonzalez, C. Ghidelli, C. C. Sheth, M. Mateos, L. Palou, and M. B. Pérez-Gago. Browning inhibition and microbial control in fresh-cut persimmon (*diospyros kaki thunb.* cv. *rojo brillante*) by apple pectin-based edible coatings. *Postharvest Biology and Technology*, 112:186–193, 2016.
- [47] G. B. Seymour, L. Østergaard, N. H. Chapman, S. Knapp, and C. Martin. Fruit development and ripening. *Annual review of plant biology*, 64:219–241, 2013.
- [48] Y. Shinozaki, P. Nicolas, N. Fernandez-Pozo, Q. Ma, D. J. Evanich, Y. Shi, Y. Xu, Y. Zheng, S. I. Snyder, L. B. Martin, et al. High-resolution spatiotem-

- poral transcriptome mapping of tomato fruit development and ripening. *Nature communications*, 9(1):364, 2018.
- [49] K. L. Simpson. Chemical changes in natural food pigments. *Chemical changes in food during processing*, pages 409–441, 1985.
- [50] I. Soubry, P. Patias, and V. Tsikoukas. Monitoring vineyards with uav and multi-sensors for the assessment of water stress and grape maturity. *Journal of Unmanned Vehicle Systems*, 5(2):37–50, 2017.
- [51] S. Srivastava and S. Sadistap. Non-destructive sensing methods for quality assessment of on-tree fruits: a review. *Journal of Food Measurement and Characterization*, 12(1):497–526, 2018.
- [52] G. Stiglic, P. Kocbek, N. Fijacko, M. Zitnik, K. Verbert, and L. Cilar. Interpretability of machine learning-based prediction models in healthcare. *Wiley Interdisciplinary Reviews: Data Mining and Knowledge Discovery*, 10(5):e1379, 2020.
- [53] J. Tang, D. Sun, S. Liu, and J.-L. Gaudiot. Enabling deep learning on iot devices. *Computer*, 50(10):92–96, 2017.
- [54] R. Tharanathan, H. Yashoda, and T. Prabha. Mango (*mangifera indica l.*)âthe king of fruitsâan overview. *Food Reviews International*, 22(2):95–123, 2006.
- [55] T. F. Thien and W. S. Yeo. A comparative study between pcr, plsr, and lw-pls on the predictive performance at different data splitting ratios. *Chemical Engineering Communications*, 209(11):1439–1456, 2022.
- [56] M. Yami, T. Solomon, B. Begna, F. Fufa, T. Alemu, and D. Alemu. Source of technical inefficiency of smallholder wheat farmers in selected waterlogged areas of ethiopia: A translog production function approach. *Afr. J. Agric. Res*, 8(29):3930–3940, 2013.

- [57] L. Ye, Y. Mai, Y. Wang, J. Yuan, Y. Suo, H. Li, W. Han, P. Sun, S. Diao, and J. Fu. Metabolome and transcriptome analysis reveal the accumulation mechanism of carotenoids and the causes of color differences in persimmon (*diospyros kaki thunb.*) fruits. *Agronomy*, 12(11):2688, 2022.
- [58] I. N. Yusoff, M. A. M. Ismail, H. Tobe, K. Date, and Y. Yokota. Quantitative granitic weathering assessment for rock mass classification optimization of tunnel face using image analysis technique. *Ain Shams Engineering Journal*, 14(1):101814, 2023.
- [59] C. Zheng, A. Abd-Elrahman, and V. Whitaker. Remote sensing and machine learning in crop phenotyping and management, with an emphasis on applications in strawberry farming. *Remote Sensing*, 13(3):531, 2021.